Capillary Breakup of Discontinuously Rate Thickening Suspensions

Pawel J. Zimoch,* Gareth H. McKinley, and A. E. Hosoi
Hatsopoulos Microfluids Laboratory, Department of Mechanical Engineering, Massachusetts Institute of Technology, Cambridge, Massachusetts 02139, USA
(Dated: April 12, 2013)

Using Discontinuously Rate Thickening Suspensions (DRTS) as a model system, we show that Beads-on-a-String morphologies can arise as a result of external viscous drag acting during capillary-driven breakup of a non-Newtonian fluid. To minimize the perturbative effect of gravity, we developed a new experimental test platform in which the filament is supported in a horizontal position at the surface of an immiscible oil bath. We show that the evolution of thin DRTS filaments during the capillary thinning process is well-described by a set of 1-dimensional (1D) slender filament equations. The strongly rate-dependent rheology of the test fluid and the aspect ratio of the filament couple to control the thinning dynamics and lead to a simple criterion describing the localized arrest of the capillary thinning process and the subsequent formation of complex, high aspect ratio Beads-on-a-String structures.

Complex, high aspect ratio structures, such as strings with embedded functionalized elements (generically denoted"beads") (Fig. 1), find applications in optics [1], self-assembly [2], bioengineering [3] and custom material design [4]. Recent studies show that such structures can be created by polymerizing a liquid filament to arrest the process of capillary breakup [1]. Currently, these Beads-on-a-String (BOAS) structures are attained by exploiting complex rheological properties of polymer solutions [1, 5–7]. The factors affecting the characteristics of the resulting structures, such as size and relative placement of beads, are still not completely understood [1, 5, 8].

In this letter, we show that formation of BOAS structures can be provoked using viscous drag. Placing a filament undergoing breakup in a bath of immiscible viscous fluid results in the creation of a rich array of structures, depending on the viscometric properties of both fluids [9–11]. Here, we couple this effect with Discontinuously Rate Thickening Suspensions (DRTS) [12] to extend the lifetime of the filament and enable formation of high aspect ratio structures. The defining feature of DRTS is a sharp increase in viscosity at a critical deformation rate $\dot{\gamma}_{\text{crit}}$ (Fig. 2(b)) [13], characterized by a Weissenberg number $Wi = \dot{\gamma}_{\text{flow}}/\dot{\gamma}_{\text{crit}}$, where $\dot{\gamma}_{\text{flow}}$ is the characteristic deformation rate of the flow. DRTS are slightly shear-thinning for $Wi \ll 1$, and thickening for $Wi \gtrsim 1$.

In a slender geometry, the rate of decay of the filament diameter is set by the slowest rate process in the system [14, 15]. In DRTS, this leads to decay at a fixed deformation rate $\dot{\gamma}_{\text{crit}}$ at late times – limited by the concomitant sharp increase in viscosity – resulting in the development of a thread of axially uniform radius, which thins exponentially (Fig. 2(c)) [16, 17]. This behavior is similar to capillary breakup of viscoelastic liquids, but the underlying physical constraint on deformation rate is different [18–22]. In addition, in contrast to viscoelastic materials, DRTS exhibit no memory effects [13, 18] which significantly simplifies the problem as the state of stress depends only on the instantaneous deformation rate, and not on the accumulated strain.

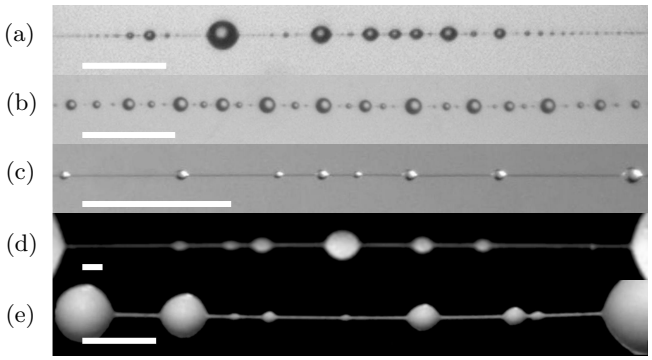

FIG. 1. Typical Beads-on-a-String (BOAS) structures. (a) Solution of poly(ethylene oxide) (PEO) in water, surrounded by air. (b) Solution of PEO in water, in corn oil bath. (c) Solution of polystyrene in styrene oil, in glycerol bath. (d) Suspension of cornstarch in glycerol, in corn oil bath. (e) Suspension of silica particles in water, in corn oil bath. Scale bars: $1mm$.

Experiments were performed with a suspension of cornstarch (argo) in glycerol (sigma, $\rho = 1.261\ kg/m^3$, $\mu = 1.4$ Pa s). The particle weight fraction was fixed at 55%. The lowest viscosity of the suspension was $\mu_0 = 15$Pas and the sharp increase in viscosity to $\mu_{\max} = 360$ Pa s occurred between $\dot{\gamma} \approx 0.1\text{-}0.5 s^{-1}$ (Fig. 2(b)). Although the dependence of DRTS rheology on mode of deformation is still not well understood [16, 17], we use the measured shear rheology with $\dot{\gamma}_{\text{crit}} \approx 0.1 s^{-1}$ as a useful proxy for understanding the behavior of these suspensions in capillary breakup.

A small amount of the suspension was placed between two rods to form an axially uniform fluid catenary. The catenary was then placed on the surface of a bath of an immiscible oil, and anchored a distance $2L$ apart, level with the surface of the oil (Fig. 2). The interfacial tension between the suspension and oil ($\sigma = 13.7\ mN/m$)

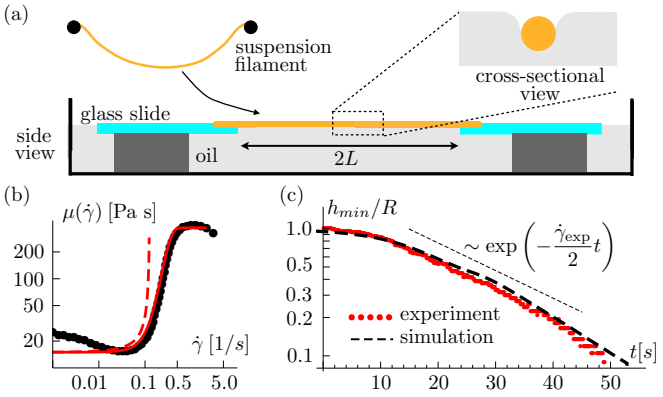

FIG. 2. (color online). (a) Experimental setup showing a DRTS catenary supported by two rods, and a floating filament attached to glass slides at both ends. The filament is held at the surface of the oil bath by surface tension. (b) Black dots: shear rheology of 55% wt. suspension of cornstarch in glycerol, measured in a parallel plate geometry. Dashed red line: constitutive relation μ_1, with $\alpha = 1$, $k = 5$ and $\dot{\gamma}_{\rm crit} = 0.1$. Solid red line: constitutive relation μ_2, with $\beta = 12$, $\xi = 1/6$, $\dot{\gamma}_{\rm crit} = 0.29$. (c) Dimensionless radius of a typical filament as a function of time, with $\dot{\gamma}_{\rm exp} = 0.1\ s^{-1}$.

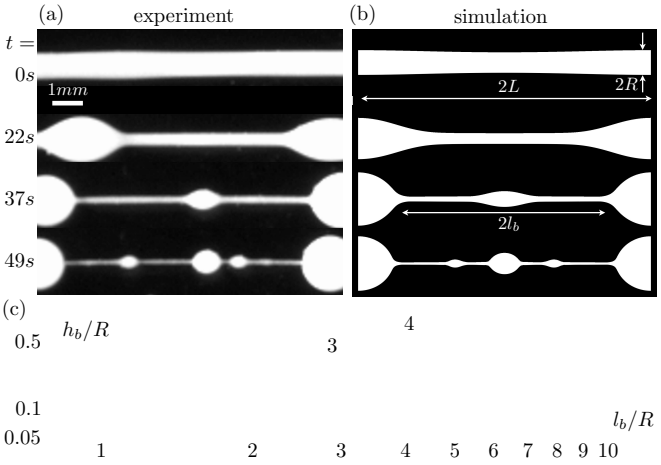

FIG. 3. (color online). (a) Experimental observations of capillary breakup of a DRTS filament (left) and (b) numerical solutions of (1)-(**??**) using μ_1 shown in Fig. 2(b), and $\lambda = 8.45$, $Wi = 10.99$ and $C_d = 0.078$ (right). (c) Dimensionless minimum radius of the filament at bead formation (h_b/R) as a function of dimensionless length of the filament (l_b/R) for external oil viscosities $\mu_{\rm high} = 3.0$ Pa s ($\triangle$) and $\mu_{\rm low} = 0.147$ Pa s ($\triangledown$).

supported the filament at the surface of the bath. Two oils of different viscosities were used: $\mu_{\rm high} = 3.0$ Pa s (Poly-Alpha-Olefin, Cannon Instrument Company) and $\mu_{\rm low} = 0.147$ Pa s (mineral oil, CVS). The initial radius of the filament R ranged between 0.5-1.5mm. Capillary breakup of the filament proceeded at the surface of the oil bath and was imaged from above. The main advantage of this method compared to typical capillary breakup instruments is that the filament remains horizontal throughout the experiment, minimizing the influence of gravity [16, 17, 23] and allowing filaments with aspect ratios of $L/R \geq 50$ to develop.

After an initial transition period, the minimum radius of the filament decreased at an exponentially decaying rate $h_{\rm min} \sim \exp(-\dot{\gamma}_{\rm exp} t/2)$ with $\dot{\gamma}_{\rm exp} = 0.1 s^{-1}$, which is consistent with the onset of thickening in shear (Fig. 2(b,c)). Subsequently, a small bulge appeared in the center of the filament, and grew to become a small droplet ("bead") (Fig. 3(a)). The radius in the thinnest section of the filament continued decaying exponentially, until $h_{\rm min} \approx 10$ particle diameters ($\approx$ 200-300 μm), at which point the filament ruptured. For long filaments, second, third and fourth generation beads appeared on the filament in a symmetrical arrangement about the central primary bead (Figs. 1(d), 3(a)). While the results reported in this letter are for a 55% wt. suspension of cornstarch in glycerol, similar behavior was observed in rate-thickening suspensions of cornstarch and silica in various water-glycerol mixtures.

The geometry of the filament at the time of bead formation, that is when $dh/dt = 0$ at the center of the filament, can be characterized by the smallest radius of the filament h_b at that time and its length $2l_b$, as measured between the two bounding drops. For experiments with filaments of various lengths in an oil of viscosity $\mu_{\rm high} = 3.0$ Pa s, h_b and l_b are related through a power-law with exponent 3/4 (Fig. 3(c)). In oil of much lower viscosity, $\mu_{\rm low} = 0.147$ Pa s, the filament radius at bead formation for a given filament length was smaller than in the more viscous oil, and the correlation between h_b and l_b was much weaker. This weaker correlation between h_b and l_b for lower viscosity oil resulted from a relative increase in importance of the details of the microstructural arrangement of the particles at small filament radii. As this microstructure could not be controlled, it remains a source of noise in the experiments [24].

To model formation of the bead structures, we consider a long, axisymmetric filament with initial radius R and length $2L$, made of fluid of constant density ρ and rate-dependent viscosity $\mu(\dot{\gamma})$, where $\dot{\gamma} = \sqrt{(\underline{\underline{\dot{\gamma}}} : \underline{\underline{\dot{\gamma}}})/2}$ and $\underline{\underline{\dot{\gamma}}}$ is the rate-of-strain tensor (Fig. 4). The filament is submerged in a bath of immiscible Newtonian fluid of density $\rho_{\rm env}$ and viscosity $\mu_{\rm env}$. The interfacial tension between the two fluids is σ. We use a cylindrical coordinate system, with origin at the center of the filament. The radius of the filament is denoted by $h(z,t)$ with initial conditions $h(z, t = 0) = R(1 - \epsilon(1 + \cos(\pi z/L))/2)$, where $\epsilon \ll 1$ and $R \ll L$. Under these conditions, the filament is unstable and the initial disturbance grows at a characteristic rate $\dot{\gamma}_{inst} = \sigma/(\mu_0 R)$. To describe the evolution of the slender filament, we use 1D approximations to the momentum and mass balance equations, derived for Newtonian filaments by Eggers and DuPont [25], and

successfully adapted for shear-thinning filaments [26]. In our experiments, the Ohnesorge number, a measure of relative importance of viscous and inertial effects in surface tension driven flows, is $Oh = \mu_0/\sqrt{\rho\sigma R} \approx 70$. Thus, neglecting inertia, the dimensionless versions of the governing equations are

$$0 = \frac{\partial}{\partial z}\left[T(z)\right] - C_d v, \quad 0 = \frac{\partial h^2}{\partial t} + \frac{\partial}{\partial z}\left(h^2 v\right). \qquad (1)$$

In nondimensionalizing these equations characteristic scales were chosen as R (length), $\Lambda = \dot{\gamma}_{inst}^{-1}$ (time) and $V = R/\Lambda$ (velocity). For convenience, from now on we consider dimensionless quantities only, and drop the tildes. The total dimensionless tension in the filament cross-section is given by $T(z) = h^2\left(\kappa + 3\mu\left(\dot{\gamma}\right)\partial v/\partial z\right)$, with

$$\kappa = \frac{1}{h\sqrt{1+h'^2}} + \frac{h''}{(1+h'^2)^{3/2}}, \qquad (2)$$

where prime represents differentiation with respect to z [6] [27]. We investigated two models for the viscosity of the suspension: the first model, $\mu_1(\dot{\gamma}) = \mu/\mu_0 = \frac{1}{k}\left[(\sqrt{3} - Wi\,\dot{\gamma})^{-\alpha} + (\sqrt{3} + Wi\,\dot{\gamma})^{-\alpha} - 2\right] + 1$ diverges as $\partial v/\partial z \to Wi^{-1}$ with parameters k and α controlling the steepness of the divergence [28]; the second model, $\mu_2(\dot{\gamma}) = \beta\left[\mathrm{erf}\left(\xi\left(Wi\,\dot{\gamma} - \sqrt{3}\right)\right) + \mathrm{erf}\left(\xi\left(-Wi\,\dot{\gamma} - \sqrt{3}\right)\right) - 2\,\mathrm{erf}(-\xi)\right] + 1$, where β and ξ are adjustable parameters, closely follows the experimentally measured constitutive relation, and does not diverge (Fig. 2(b)).

The model μ_1, which is amenable to theoretical analysis, assumes that the dimensionless elongation rate of the filament may never exceed Wi^{-1}, regardless of the applied stress. The limitations of this simplified model are investigated by comparing it to the more accurate model μ_2, which is too complex for analytical consideration, but can be implemented in numerical simulations.

The evolution equations and boundary conditions contain three dimensionless groups: Wi, C_d, and λ which is the distance from the center of the filament to the base of the bounding drop, and can be approximated as $\lambda = L - (3/2L)^{1/3}$, where $2L$ is the dimensionless initial length of the filament (Fig. 4).

If $\mu_0 \gg \mu_{\mathrm{env}}$, which is the case in our experiments, the filament acts like a rigid rod translating along its axis, and the drag coefficient can be derived from slender body theory [11, 29]. Thus, the coefficient of drag exerted on the filament by the outer fluid is defined as $C_d = 2\mu_{\mathrm{env}}/(\mu_0 \ln(\lambda/h_{\min}))$. In this regime, the viscosity of the external fluid has a negligible effect on the initial instability of the filament, but becomes significant when $h_{\min} \ll 1$.

Equations (1) were solved for an initially stationary filament, subject to symmetry and no-flux boundary conditions on the domain $\langle 0, L\rangle$ with an upwinded finite volume scheme using Newton's method, for both constitutive relation models. The evolution of the filament shape

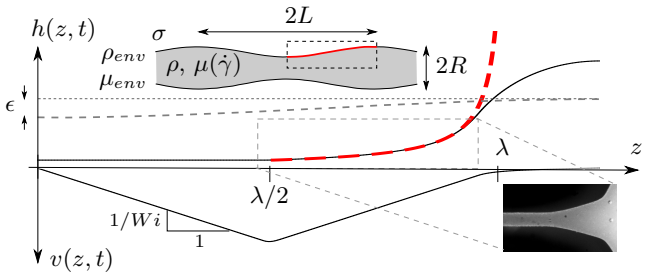

FIG. 4. (color online). Initial (thin, dashed) and late-time (solid) filament shapes and velocity fields from a numerical solution of (1) with $C_d = 0$ and $\lambda/Wi < 2/3$. Thick dashed line represents theoretical shape in domain $\langle\lambda/2, \lambda\rangle$. The solution domain is enclosed in the dashed rectangle in the upper inset. Relative size of the initial disturbance ϵ is exaggerated for clarity. The velocity field reaches a steady state, where the velocity gradient $\partial v/\partial z$ is limited to $\pm Wi^{-1}$ in the region $\langle 0, \lambda\rangle$. Lower inset: experimental photograph.

along with corresponding experimental images are shown in Figures 2(c) and 3(a,b).

As expected, the filament initially evolves as a Newtonian fluid, but eventually transitions to an exponentially decaying rate $h_{\min} \sim \exp(-t/(2Wi))$ (Fig. 2(c)), due to the rapid increase in viscosity at $\partial v/\partial z \approx Wi^{-1}$. The deviation from Newtonian behavior occurs when the viscous stress $\tau = \mu(\dot{\gamma})\,\partial v/\partial z$ in the filament reaches Wi^{-1}, and $|\partial v/\partial z| \approx Wi^{-1}$ (Fig. 4).

A bead begins to form when the deformation rate at the center of the filament becomes smaller than the deformation rate in other parts of the filament, namely when the viscous stress at the center of the filament decreases below Wi^{-1}. When this happens, a small bulge appears in the middle of the filament due to volume conservation. This leads to a reversal in the direction of the net surface tension force, which drives flow towards the bulge, leading to formation and growth of the first bead. Therefore, the first bead forms at the center of the filament when $3\mu(\dot{\gamma})\dot{\gamma}|_{z=0} = 3Wi^{-1}$. To relate this criterion to the observable aspect ratio $\lambda/h_{\min}$ of the thinning filament, we consider the evolution of a filament with constitutive relation μ_1.

For $C_d = 0$ and μ_1, simulations show that the viscous stress inside the filament attains a steady value $\tau_{\max}$ at late times, in contrast to Newtonian fluids and polymer solutions, where the stress inside the filament grows as $\sim h_{\min}^{-1}$ [6]. The rescaled value of this maximum viscous stress $\tau_{\max}\lambda$ can be represented as a function of a single parameter λ/Wi. For $\lambda/Wi < 2/3$ we find $3\tau_{\max}\lambda \approx 2$ and for $\lambda/Wi > 2/3$ we find $\tau_{\max}\lambda \sim \lambda/Wi$ [30]. These two predicted regimes and the threshold value $\lambda/Wi \approx 2/3$ are captured by simulations (Fig. 5).

Next, we evaluate the variation in $T(z)$ when $C_d \neq 0$. For $\lambda/Wi < 2/3$, the filament velocity eventually reaches steady state in which the velocity for $0 < z < \lambda/2$ is given

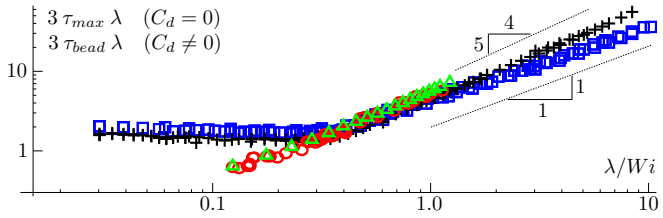

FIG. 5. (color online). Comparison of simulation and experimental results. Blue squares: simulations with μ_1, $C_d = 0$. Black crosses: simulations with μ_1 and $C_d \neq 0$. Green triangles: simulations with μ_2 and $C_d \neq 0$. Red Circles: experimental results; each mark represents formation of the first, central bead. The value of the ordinate is $3\tau_{\max}\lambda$ for simulations with $C_d = 0$, and $3\tau_{\text{bead}}\lambda$ for simulations with $C_d \neq 0$ and for experiments.

by $v = Wi^{-1}z$ (Fig. 4). Substituting this expression into equation (1) and integrating yields

$$T(z)|_0^{\lambda/2} = \int_0^{\lambda/2} C_d Wi^{-1} z dz = \frac{1}{2} C_d Wi^{-1} \left(\frac{\lambda}{2}\right)^2. \quad (3)$$

Since $h = h_{\min}$ in this region, substituting equation (2) into (3) leads to

$$3\mu(\dot{\gamma})\dot{\gamma}|_{z=0}^{z=\lambda/2} = \frac{1}{2} C_d Wi^{-1} \left(\frac{\lambda}{2h_{\min}}\right)^2. \quad (4)$$

The beading criterion may thus be expressed as

$$3\mu(\dot{\gamma})\dot{\gamma}|_{z=\lambda/2} = 3\tau_{\text{bead}} = \frac{1}{2}\frac{C_d}{Wi}\left(\frac{\lambda}{2h_{\min}}\right)^2 + \frac{3}{Wi}. \quad (5)$$

We relate τ_{bead} to $\tau_{\max}$ via $\tau_{\text{bead}} \approx \tau_{\max} f(\lambda)$ where $f \leq 1$, and f depends on the shape of the filament. We expect the rescaled viscous stress at bead formation $\tau_{\text{bead}}\lambda$ to collapse on the curve formed by $\tau_{\max}\lambda$ in Figure 5, with a possible positive deviation due to $f(\lambda)$. This is indeed the case, and the numerical results show that $f(\lambda) \approx 1$ for $3\lambda < 2Wi$ and $f(\lambda) \sim \lambda^{-1/4}$ for $3\lambda > 2Wi$ (Fig. 5).

The rescaled stress at bead formation $3\tau_{\text{bead}}\lambda$ for simulations using constitutive relation μ_2, plotted in Figure 5 for parameters corresponding to our experiments, shows significant variaton from simulations using μ_1 for $\lambda/Wi < 2/3$. The reason for this discrepancy is that, under the simplified viscosity model μ_1, the deformation rate may not exceed Wi^{-1}, and the viscous stress is unbounded. As a result, the stress inside the filament becomes dependent on λ for short filaments and relatively fast drainage rates. However, in a real suspension the viscosity increases in a more gradual way, and the deformation rate continues to increase slowly throughout the filament's evolution. This is reflected in simulations using the more realistic viscosity model μ_2, which allows for a gradual increase in deformation rate, and limits the viscous stress.

The beading criterion expressed in terms of experimental variables is

$$3\tau_{\text{bead}}\lambda = \left(\frac{\mu_0}{2\mu_{\text{env}}\ln(l_b/h_b)}\left(\frac{l_b}{2h_b}\right)^2 + 3\right)\frac{\dot{\gamma}_{\text{exp}}}{\sigma/\mu_0 R}\frac{l_b}{R} \quad (6)$$

The additional factor of 1/2 in front of the drag term in equation (6) accounts for only half the circumference of the thinning filament being exposed to the outer fluid in the experiments. The experimental data for μ_{high}, shown in Figure 3(c) is replotted in Figure 5 using equation (6), showing satisfactory agreement with simulations using constitutive relation μ_2.

In conclusion, the viscous drag force from an external fluid can be used in capillary breakup processes to generate complex high-aspect-ratio structures, such as Beads-on-a-String. In general, surface tension-driven instabilities can be used to generate complex geometries at small scales [8, 31] and allow use of efficient microfluidic techniques for processing [32]. The ability to exploit external viscous drag to influence the process of bead formation is not specific to DRTS. As Figure 1 shows, the same principle can be used to provoke bead formation in polymer solutions. Understanding the effect of drag in the context of viscoelastic polymer dynamics, however, requires analysis more complex than presented here. Finally, we note that, despite recent progress, behavior of rate thickening suspensions remains poorly understood in flows other than simple shear. The experimental method developed in this study allows easy characterization of DRTS in flows dominated by elongation, raising the possibility of investigating the rate-thickening effect in more general kinematics.

* pzimoch@mit.edu

[1] S. Grilli, S. Coppola, V. Vespini, F. Merola, A. Finizio, and P. Ferraro, Proceedings of the National Academy of Sciences **108**, 15106 (2011).
[2] K. C. Cheung, E. D. Demaine, J. R. Bachrach, and S. Griffith, IEEE Transactions on Robotics **27**, 718 (2011).
[3] B. K. Brettmann, S. Tsang, K. M. Forward, G. C. Rutledge, A. S. Myerson, and B. L. Trout, Langmuir **28**, 9714 (2012).
[4] E. Brown, A. Nasto, A. G. Athanassiadis, and H. M. Jaeger, Physical Review Letters **108**, 108302 (2012).
[5] P. P. Bhat, S. Appathurai, M. T. Harris, M. Pasquali, G. H. McKinley, and O. A. Basaran, Nature Physics **6**, 625 (2010).
[6] C. Clasen, J. Eggers, M. A. Fontelos, J. Li, and G. H. McKinley, Journal of Fluid Mechanics **556**, 283 (2006).
[7] M. S. N. Oliveira, R. Yeh, and G. H. McKinley, Journal of Non-Newtonian Fluid Mechanics **137**, 137 (2006).
[8] R. Sattler, C. Wagner, and J. Eggers, Physical Review Letters **100**, 164502 (2008).

[9] S. Tomotika, Proceedings of the Royal Society of London Series *A*. Mathematical and Physical Sciences **150**, 322 (1935).

[10] M. Tjahjadi, H. A. Stone, and J. M. Ottino, Journal of Fluid Mechanics **243**, 297 (1992).

[11] H. A. Stone and J. R. Lister, Physics of Fluids **10**, 2758 (1998).

[12] The more commonly used name, Discontinuously Shear-Thickening Suspensions, is made more general here to account for the fact that the primary deformation mode in capillary breakup is elongation.

[13] H. A. Barnes, Journal of Rheology **33**, 329 (1989).

[14] J. Eggers, Reviews of Modern Physics **69**, 865 (1997).

[15] J. Eggers and E. Villermaux, Reports on Progress in Physics **71**, 036601 (2008).

[16] E. E. Bischoff White, M. Chellamuthu, and J. P. Rothstein, Rheologica Acta **49**, 119 (2009).

[17] M. I. Smith, R. Besseling, M. E. Cates, and V. Bertola, Nature Communications **1**, 114 (2010).

[18] G. H. McKinley and T. Sridhar, Annual Review of Fluid Mechanics **34**, 375 (2002).

[19] V. M. Entov and E. J. Hinch, Journal of Non-Newtonian Fluid Mechanics **72**, 31 (1997).

[20] A. Fall, N. Huang, F. Bertrand, G. Ovarlez, and D. Bonn, Physical Review Letters **100**, 018301 (2008).

[21] E. Brown and H. M. Jaeger, Physical Review Letters **103**, 086001 (2009).

[22] Y. S. Lee and N. J. Wagner, Rheologica Acta **42**, 199 (2003).

[23] M. Roché, H. Kellay, and H. A. Stone, Physical Review Letters **107**, 134503 (2011).

[24] See Supplementary Materials.

[25] J. Eggers and T. F. Dupont, Journal of Fluid Mechanics **262**, 205 (1994).

[26] O. A. Basaran and O. E. Yildirim, Chemical Engineering Science **56**, 211 (2001).

[27] Note that $\kappa/2$ is not the mean curvature. While $\tilde{h}''$ is asymptotically negligible in the slender filament limit, it is often retained in capillary breakup problems to enable capture of capillary structures such as beads under equilibrium conditions of no flow.

[28] Note that in elongational flow, the magnitude of the (dimensionless) deformation rate is $\tilde{\dot{\gamma}} = \sqrt{3}\partial\tilde{v}/\partial\tilde{z}$.

[29] R. G. Cox, Journal of Fluid Mechanics **44**, 791 (1970).

[30] See Supplementary Materials.

[31] P. T. McGough and O. A. Basaran, Physical Review Letters **96**, 054502 (2006).

[32] S. Pennathur, C. D. Meinhart, and H. T. Soh, Lab on a Chip **8**, 20 (2007).